Astronomy & Astrophysics manuscript no. cr8b May 24, 2019
(DOI: will be inserted by hand later)

Cosmic Rays VIII

Models and Predictions for Cosmic Rays Origin and Propagation

A. S. Popescu[1], P. L. Biermann[2], and N. Langer[3]

[1] Astronomical Institute of Romanian Academy of Science, Str. Cutitul de Argint 5, RO-040557 Bucharest, Romania
e-mail: sabinp@aira.astro.ro
[2] Max-Planck Institute for Radioastronomy, D-53121 Bonn, Germany
e-mail: plbiermann@mpifr-bonn.mpg.de
[3] Astronomical Institute, Utrecht University, Princetonplein 5, 3584 CC, Utrecht, The Netherlands
e-mail: N.Langer@astro.uu.nl

Received/Accepted

Abstract. It is presumed that the observed cosmic rays up to about $3 \cdot 10^{18}$ eV are of Galactic origin, the particles being the ones which are found into the composition of the stellar winds of stars that explode as supernova into the interstellar medium (ISM) or into their winds. These particles are accelerated in the supernova shock. In order to obtain the observed cosmic ray spectrum it is necessary to take into account the diffusive losses in the Galaxy (which are making the energy spectrum more steeper). Another modification of the source spectrum is due to the fragmentation (spallation) of the cosmic ray particles in their collision with particles of the interstellar medium (ISM). In this paper we are proving that some particles are injected in the supernova shock one or two time ionised, and, also, that the contribution to the cosmic ray massive stars ($30M_{\odot} \leq M \leq 50M_{\odot}$) accelerated particles (where the winds are highly enriched in heavy elements) to cosmic ray accelerated particles from stars with $15M_{\odot} \leq M \leq 30M_{\odot}$ is 1:2 for elements with $Z \geq 6$.

Key words. cosmic rays – stars: abundances – supernovae: individual: shock acceleration and FIP correction

1. Introduction: What are Cosmic Rays

In 1912, in Austria, after observing the discharging behavior of electroscopes during a balloon ascent, the physicist V.F. Hess concluded that "a radiation of very great penetrating power enters our atmosphere from above". In 1936 Hess shared a Nobel Prize in physics for the discovery of cosmic rays. The cosmic radiation which impinges upon the atmosphere of the earth consist mostly of fast protons and alpha particles. Because of their net charge, the cosmic rays gyrate in magnetic fields. In a reference frame with no electric field:

$$\frac{d\mathbf{p}}{dt} = \frac{Ze}{c}(\mathbf{v} \times \mathbf{B}),$$

Here $\mathbf{p} = \gamma m\mathbf{v}$ is the relativistic momentum, with $\gamma = 1/\sqrt{1-(\mathrm{v}/c)^2}$, $\mathbf{v}$ is the velocity, Ze the charge, and m the rest mass of the particle. For circular motion, $\mathbf{v}$ only changes direction, so:

$$\frac{dp}{dt} = \left(\frac{p}{\mathrm{v}}\right)\left(\frac{d\mathrm{v}}{dt}\right),$$

$$= \frac{p\mathrm{v}}{r}.$$

Therefore, in the extreme relativistic limit:

$$\frac{pc}{Ze} = rB,$$

where pc is the energy ϵ, and:

$$\frac{\epsilon}{ZrB} = 300 \text{ eV/gauss} \cdot \text{cm}.$$

The ratio $\frac{pc}{Z}$ is called *rigidity*. Thus, although the cosmic rays travel at essentially the speed of light, their net drift motion through cosmic magnetic fields is much slower; because the fields are tangled and dynamic, this motion has the character of a random walk.

Cosmic rays are particles, which have been accelerated in the Galaxy or into the extragalactic space. They come as electrons, protons, heavier nuclei, and their antiparticles. In the radiation were detected almost all the elements of the periodic table as well as their isotopes. Only those particles are missing, that decay with a lifetime generally too short to be observed on Earth, like neutrons and many radioactive isotopes. The energy spectrum reaches from some MeV to 10^{20} eV/particle, the highest energy of any known radiation. From the lower end up to the highest energies the flux decreases by about 30 orders of magnitude. In consideration of such a large energy range, different detection techniques are necessary to explore the cosmic radi-

ation. Methods used at medium and high energy ($< 10^{10}$ eV) require detectors carried on balloons, rockets or sattellites and for studying the charged component of the cosmic radiation this technique has been extended up to several 10^{14} eV/particle. At still higher energies the observations are done with detectors located deep underground and air shower arrays which cover the ultra high energy (UHE; $> 10^{14}$ eV) and extremely high energy (EHE)-regions ($> 10^{18}$ eV). Whereas the lower energy experiments at the top of the atmosphere measure the primary nuclei directly, the ground-based arrays only detect the air showers generated by the incoming particles.

Up to now, the origin and acceleration processes are still subjects of debate. As the main sources supernovae, quasars, active galactic nuclei (AGN) and Gamma Ray Bursts (GRB) are assumed. The charged particles of the cosmic ray radiation appear nearly isotopic on earth, because they are deflected in the interstellar magnetic fields and so only the neutral constituents such as photons and neutrinos would provide direct information on their acceleration site. The energy content of the cosmic ray radiation is about 1 eV/cm^3 and therefore comparable with other forms of energy in our galaxy, like magnetic fields ($\sim$ 1 eV/cm^3) or starlight ($\sim$ 0.44 eV/cm^3).

There are now two main proposals to explain the origin of cosmic rays. One concept traces the injection to dust particles, and the initial acceleration up to the knee to supernova explosions in the interstellar medium, and the further acceleration to a stochastic mechanism between irregularities in the interstellar medium (Drury et al. 1999; Drury et al. 2003; Meyer er al. 1997; Zirakashvili et al. 1996). The second concept traces the injection and acceleration to shocks running through massive star winds, with most of the spallation taking place in the wind shells. In this concept the acceleration does reach up to 3 EeV, for Fe nuclei. In the first concept the knee derives from the acceleration limit of supernova shocks in the ISM; in the second concept the knee derives from a scale change in the shocks, when the drift acceleration becomes inefficient, and so the slope gets steeper. The data imply from the relative sharpness of the knee, that the acceleration limit in the ISM is very sharply defined in the first concept, and in the second concept requires that all very massive stars look internally very much the same at the time of explosion. In this paper we continue to explore the various checks necessary for the second concept.

2. Origin and Propagation of Cosmic Rays

2.1. Origin of Cosmic Rays

Recently three source sites have been proposed for the observed cosmic rays (Wiebel-Sooth et al. 1998):

1. Supernova explosions into the interstellar medium, or ISM-SNe. This component produces mostly hydrogen and the observed energetic electrons up to about 30 GeV, and dominates the *all particle* flux up to about 10^4 GeV.
2. Supernova explosion into predecessor stellar wind, or wind-SNe. This component produces the observed electrons above 30 GeV, helium and most heavier elements already from GeV particle energies. Due to a reduction in acceleration efficiency at a particular rigidity the slope increases, thus producing the knee feature. The component extends ultimately to several EeV. Since the winds of massive stars are enriched late in their life, this component shows a heavy element abundance which is strongly increased over that of the ISM.
3. Powerful radio galaxies produce a contribution which dominates beyond about 3 EeV, and consist mostly of hydrogen and helium, with only little addition of heavy elements. At this energy the interaction with the microwave background cuts off the contribution from distant extragalactic sources, the Greisen-Zatsepin-Kuzmin (GZK) cutoff. There are a small number of events which appear to be beyond this energy, and whether they fit into such a picture is open at present.

The theory was originally proposed in Biermann (1993a, paper CR I) and in Rachen & Biermann (1993, paper UHE CR I). Various tests were performed in Biermann & Cassinelli 1993, paper CR II; Biermann & Strom 1993, paper CR III; Stanev *et al.* 1993, paper CR IV etc.

2.2. Cosmic Rays up to $3 \cdot 10^{18}$ eV

The Cosmic Rays spectrum at GeV energies is close to $E^{-2.75}$, and at higher energies close to $E^{-2.65}$ below the "knee" at $\approx 5 \cdot 10^{15}$ eV, from where the spectrum turns down to about $E^{-3.1}$, to flatten out again near $3 \cdot 10^{18}$ eV (the "ankle"). The chemical composition is roughly similar to that of the interstellar medium, with reduced hydrogen and helium relative to silicon, and with some general enhancement of elements of low first ionization potential as we find in solar energetic particles. The low energy end of the observed spectrum is cut off due to the interaction with the solar wind is at around few hundred MeV. There is a reason to believe that in the interstellar space, outside the Solar system, the cosmic ray spectrum extends down to 30 - 60 MeV (Nath & Biermann 1994).

The theory which claims to account for the origin of cosmic rays below $3 \cdot 10^{18}$ eV traces them to the shockwaves caused by supernovae exploding either into the interstellar medium, either into the predecessor stellar wind.

2.3. Cosmic Ray Acceleration

Cosmic rays with energies up to 100 TeV are thought to arise predominantly through shock acceleration by supernova remnants (SNR) in our Galaxy. A fraction of the accelerated cosmic rays should interact within the supernova remnant and produce gamma-rays. Recent observations above 100 MeV by the EGRET instrument on the Compton Gamma Ray Observatory have found gamma ray signals associated with at least two supernova remnants - IC 443 and γ Cygni (however, it is possible that the gamma ray emission from γ Cygni to be associated with a pulsar within the remnant rather than the remnant itself). Further evidence for acceleration in SNR comes from the

recent ASCA observation of non-thermal X-ray emission from SN 1006. Reynolds (1996) and Mastichiadis (1996) interpret the latter as synchrotron emission by electrons accelerated in the remnant up to energies as high as 100 TeV, although Donea and Biermann (1996) suggest it may be bremsstrahlung from much lower energy electrons.

Acceleration to somewhat higher energies than 100 TeV may be possible, but probably not high enough to explain the smooth extension of the spectrum to 1 EeV. Several explanations for the origin of the cosmic rays in this range have been suggested: reacceleration of the supernova component while still inside the remnant; by several supernovae exploding into a region evacuated by a pre-supernova star; by acceleration in shocks inside the strong winds from hot stars or groups of hot stars. At 5 EeV the spectral slope changes, and there is evidence for a lightening in composition and is likely this marks a change from galactic cosmic rays to extragalactic cosmic rays.

For stochastic particle acceleration by electric fields induced by motion of magnetic fields B, the rate of energy gain by relativistic particles of charge Ze can be written (in SI units):

$$\left(\frac{dE}{dt}\right)_{acc} = \xi Zec^2 B$$

where $\xi < 1$ and depends on the acceleration mechanism.

The 2nd order Fermi acceleration (Fermi's original theory) can be modified in the context of supernova shocks, or other strong astrophysical shocks, into the more efficient 1st order Fermi mechanism at supernova (SN) or other shocks (Protheroe 1996).

3. Propagation of Galactic Cosmic Rays

3.1. The FIP Factor Correction

The elemental and isotopic mass fractions of cosmic rays when traced back to their sources resemble general mass fractions (or with the general abundances - GA) of elements, as those in Fig. 1, but display also some significant differences. The general mass fractions are based mainly on measurements of solar spectra and in carbonaceous chondrite meteorites. For the elements H, He and N the difference between CR and GA are factors of 20-30; they are underabundant in cosmic rays. The elements O, S, and Ar are underabundant in CR by a factor of about 4 and the nuclide ^{20}Ne by a factor of about 6. The elements C and Zn and the nuclide ^{22}Ne are underabundant by a factor of about 2.

The cosmic ray source abundances of elements and isotopes are deduced from the abundances of cosmic rays near Earth, applying propagation corrections for the secondary components produced by **nuclear spallation** in the interstellar gas.

The cosmic ray source composition resembles that of normal stars like the Sun, modified by the photosphere, chromosphere to corona particle escape mechanism that result in a diminished element abundance for the elements whose first ionization potential (FIP) exceeds about 10 eV. The Fig. 1 shows the ratios of cosmic-ray source abundances to general abundances (so, for acceleration of CR in the ISM model), normalized at Si, plotted as a function of FIP. We note that FIP provides a partial organizing principle of the CR abundances relative to GA. The value of about 10 eV implies a first-stage injection temperature (at stellar photospheres) of $\sim 10^4$ K (about 1 eV), with easier escape for the charged ones. When these particles become coronal particles, they are boosted up to energies near 1 keV. Some of the coronal particles are boosted up in energy, becoming flare particles, with energies of the order of 1 MeV. A further stage of injection (stellar flare particles near the shock waves of supernova remnants) at energies near 1 MeV is plausible, as relative ionization loss effects on particle range and on the composition cancels due to the effective charges of atoms near energies of 1 MeV/nucleon.

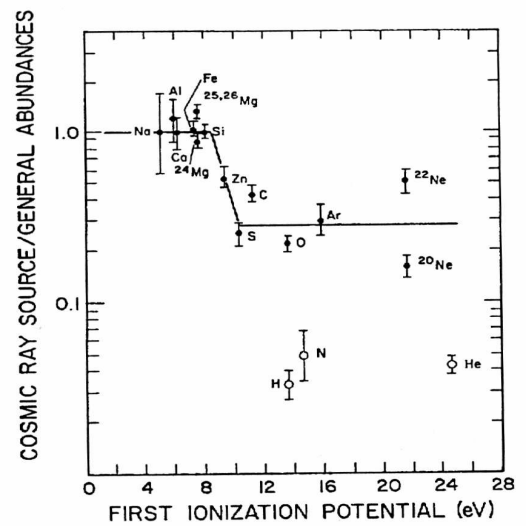

Fig. 1. The ratio of CR source abundances to the general abundances (Silberberg & Tsao 1990)

It is to be noted that the elements (and isotopes of Ne) with FIP > 10 eV have a very wide spread, and that other organizing principles in addition to FIP are needed. Since ^{22}Ne, C and O in cosmic rays contain contributions from Wolf-Rayet stars, and Ne could be affected by suppression of light elements it is useful to adopt the elements S and Ar for the FIP correction. A value of $I = 0.27$ for FIP $\geq$ 10.4 eV is adopted, and $I \equiv 1$ for FIP $\leq$ 8.4 eV. We note that Zn, with FIP = 9.4 eV, is in the middle of the transition region. Other forms (e.g. linear) have been proposed for the FIP correction. A linear fit it is still unsatisfactory (as seen in Fig. 1), especially for N and ^{22}Ne.

3.2. Contribution of Wolf-Rayet Stars to the Composition of Cosmic Rays

A second difference between the cosmic ray source composition and the general abundance is the enhancement of ^{22}Ne, ^{25}Mg and ^{26}Mg. Prantzos et al. (1985) showed that the abundance ratio C/O in cosmic rays (about twice the solar one) can be explained in terms of Wolf-Rayet star contribution to carbon. The winds of Wolf-Rayet stars are energetic, close to 0.1 MeV/nucleon, relatively close to the energies of flare particles and so, the acceleration of these wind particles is possible. The Wolf-Rayet stars go through two phases: WN,

when N produced in CNO hydrogen-burning cycle is abundant at the stellar surface, and WC, when C, produced in helium burning is abundant at the surface, and ^{14}N burns into ^{22}Ne (Silberberg & Tsao 1990).

3.3. Spallation Correction

The spallation is one of the processes that has one of the most important roles in the modification of the abundance of cosmic rays in their transportation through ISM.

The basic features of target fragmentation, sometimes called "spallation", are very well understood: heavy fragments arise from peripheral collisions of heavy ions or relativistic protons with the target nucleus. These so called "spectators" of the reaction are excited primary fragments which then decay into the final fragments by a sequence of evaporation steps.

The spectrum of the residual nuclei seems to be determined to large extent, but not fully, by the evaporation process.

The difference between the spallation in high-energy physics in accelerators and in astrophysics is that, in the first case, the targets are the nuclei and the projectiles are the high-energy protons and in the second case the targets are the ISM protons (in first approximation) and the projectiles are the nuclei that form the cosmic radiation. So everything depends just on which particle is put into the reference frame. About 10% by number of the interstellar gas is helium. Hence, about 20% of cosmic ray generated nuclear spallation nuclear products are formed in nucleus-helium interactions. In the analysis of cosmic ray interactions with atmospheric nuclei (mainly nitrogen and oxygen) an accurate knowledge of nucleus-nucleus interactions becomes essential (Tsao et al. 1998).

High-energy protons cause many different nuclear reactions and, in principle, all these nuclear processes have to be taken into account for a proper description of the total process. Possible outgoing particles are, for example, all light particles, gamma rays and (above incident energies of 150 MeV) pions. Furthermore, high-energy fission may occur and outgoing particles from the proton bombardment stage further reactions. Clearly, a wide spectrum of reaction products will be formed. Because of this diversity, the nuclear data needs for accelerator-based transmutation have been categorized in the following classes:

1. *Proton-induced reaction data*
   High-energy proton reactions represent the primary step of the total transmutation or spallation process, and the importance of nuclear data associated with these reactions is obvious. Also secondary protons with lower energy than the bombarding energy are involved. Needed data include total, elastic, inelastic, spallation cross sections, fission cross sections and reaction cross sections for outgoing light particles (p, n, d, t, α, γ, π^+, π^0, π^-) and fission products. In particular, total neutron and proton production cross sections are relevant. Energy-angle distributions are mainly required for outgoing high-energy neutrons and protons. Cross-sections for outgoing protons or neutrons constitute the most important data. For the method based on intense neutron fluxes, (p, xn) data have highest priority, but also the total proton, neutron and spallation yields are required.

2. *Neutron-induced reaction data*
   After the interaction of a high-energy proton with a target nucleus, high-energy neutrons which have been knocked out by the intranuclear cascade will induce secondary nuclear reactions in the actinides and/or fission products and in the spallation target. The same data as needed for proton-induced reactions are required for these high-energy neutrons. The highly excited residual nucleus that is left after the intranuclear cascade also evaporates a large number of relatively low-energy neutrons. The low-energy reactions that are induced by these outgoing neutrons have been subject to extensive evaluations. The additional neutron-induced data that are required are therefore mainly those for energies between 20 and 1500 MeV.

3. *Other nuclear reaction data*

The spallation happens when the supernova shock travels through the stellar wind and then hits the surrounding molecular shell of dense gas. Then, there are two ways to consider the spallation: first, in the approximation that the spallation is steady, and second, that the spallation is taking place in an expanding medium with a time scale of expansion comparable to the time scale of the spallation.

4. The Initial Mass Function (IMF)

The IMF is assumed to be a time invariant mass spectrum with a power low of the form:

$$n(m)dm \propto m^{-(1+x)}dm$$

for which m is the mass of a main sequence (MS) star in units of $M_\odot$, $m_l \leq m \leq m_u$ and $n(m)dm$ - the number of stars in the mass interval m and $m+dm$; m_l is a lower mass limit of stars, and m_u is the upper limit of stars. Normally, the IMF is derived from the observed present-day mass function (PDMF) in the solar neighborhood, which is assumed to be independent of time. The derivation of the IMF from PDMF is difficult, involving assumptions about the star formation rate during the lifetime of the Galaxy. For stars with lifetimes longer than the age of the Galaxy ($m \leq 1M_\odot$), IMF is derived by assuming an average star formation rate in the past, whereas for stars with lifetimes negligible relative to the age of the Galaxy ($m \geq 2M_\odot$), the IMF is derived by assuming a present-time formation rate and taking into account the stellar lifetimes ($\tau(m)$). Given the uncertainties in both theory and observation, the IMF variations can be parameterized, and the proposed IMF can be tested by means of a detailed chemical evolution model. This method has been adopted in many cases. Globular clusters are expected to have a IMF similar to the Miller-Scalo form, with a typical lower mass limit of 0.1 $M_\odot$. The Miller-Scalo IMF can be well approximated by a half-Gaussian distribution in $\log m$, which is:

$$\phi(\log m) = C_0 \exp[-C_1(\log m - C_2)^2],$$

where $C_0 = 66.2$, $C_1 = 1.15$, $C_2 = -0.88$ (Lu et al. 2001).

5. Chemical Yields for MS and post-MS Stars

To have acceleration of wind particles in a supernova shock, first it is necessary to have a star massive enough to make possible the explosion like supernova but also to have, in their pre-supernova stage strong winds to enrich the circumstellar medium with heavy elements.

In the Hertzsprung-Russell diagram, stars along the main sequence need to be considered in four separate zero age mass ranges:

- Stars below about 8 $M_\odot$ do not explode as supernovae;
- Stars from about 8 to about 15 $M_\odot$ explode as supernovae, but do not have a strong stellar wind, and so explode into the interstellar medium. In pre-supernova stage evolve as Red Supergiants (RSG);
- Stars from about 15 to 30 $M_\odot$ have a substantial wind. This wind is enriched only in helium. The chemical composition of the wind at the time of explosion is approximately 50% in He and 50% in H. The mass in the shell of wind-swept material is moderate. In pre-supernova stage evolve as RSG;
- Stars from about 30 $M_\odot$ have strong winds. This wind is enriched in heavy elements and has little hydrogen left. The mass in the shell of wind-swept material is large. In pre-supernova stage evolve as Wolf-Rayet (WR) stars or as "luminous blue variables" (LBV) stars.

The evolution of massive stars depends strongly on mass loss by stellar winds (Heger et al. 2003). The most illustrative example is given by the fact that massive stars with initial masses from 25 $M_\odot$ are likely to be left with only about 5 $M_\odot$ at the end of their Wolf-Rayet stage. Wolf-Rayet stars represent a late evolutionary stage of stars with masses of 25-50 $M_\odot$ which occurs as a result of the loss of all or at least the major part of their hydrogen-rich envelope. Although WR stars are among the most luminous stellar objects in the sky and contribute substantially to the chemical and dynamical evolution of galaxies, even their basic properties, e.g. their radii or their luminosities, are still not well known today. This arises mainly from the fact that WR stars are obscured by their own dense stellar wind, the origin of which is not yet understood and which renders the modeling of WR stars and their atmospheres difficult (Heger & Langer 1996).

Through frequently modeled, the hydrogen and helium burning stages of massive stellar evolution are greatly affected by uncertain physics: convection, mass loss (Heger et al. 2003) and the cross section for the $^{12}C(\alpha,\gamma)^{16}O$ reaction. The extent of convective penetration into regions which are stable according to local criteria ("convective overshooting") is especially uncertain. Observational arguments in favor of a moderate amount of overshooting is, for example the main-sequence widening, but those arguments are indirect, and other processes such as rotationally induced mixing or improvements in radiative opacities might satisfy the same observational constraints.

A second uncertainty concerns the efficiency of molecular weight gradients in preventing convective mixing ("semiconvection"). Two extreme assumptions are frequently seen in the literature:

1. that molecular weight barriers may be neglected altogether (the "Schwarzschild criterion"for convection);
2. that molecular weight barriers prevent almost any mixing ("Ledoux criterion" for convection).

In between these extremes, semiconvection describes the rate of mixing in regions having superadiabatic temperature gradients, but stabilized by finite molecular weight gradients.

The physics of mass loss is not sufficiently well understood for almost any evolutionary phase of massive stars to make a reliable quantitative prediction. Progress has been achieved recently in the theory of radiatively driven winds, which is applicable to the hot stages ($T_{eff} \geq 15,000$ K) of massive hydrogen-rich stars, but this still involves considerable uncertainty and does not agree with observed mass-loss rates to better than a factor of 2. Much more uncertain are the mass-loss rates for red supergiants. Only approximate fits to the observations exist and a factor of 10 uncertainty may not be an overestimate. Finally, mass-loss rates for LBVs and for the various types of WR stars are also uncertain.

6. Mass Loss and its Effects on the Chemical Yields

Mass loss by stellar winds is a dominant effect in the evolution of stars with an initial mass $M \geq 20M_\odot$. The standard picture for the pre-supernova structure of a massive star (at least near solar metallicity) is that of a red supergiant which contains a hydrogen-rich envelope of many solar masses at the time of explosion. However, the inclusion of mass loss allows several alternative structures, all of which presumably have observational counterparts as supernovae. There may be red supergiants with a very small hydrogen-rich envelope, hydrogen-rich WR stars, helium stars (WR stars with a surface helium mass fraction $Y_S = 1 - Z$, with Z as initial metallicity), or WR stars of WC or WO type, which contain large amounts of He, C and O (and no hydrogen) at their surface.

The star may become a bare core, then enter the WR stage and follow all or part of the sequence WNL (L for late), WNE (E for early), WCL, WCE and WO. This sequence corresponds to a progression in the exposition of the nuclear products: CNO equilibrium with H present (WNL), CNO equilibrium without H (WNE), early visibility of the products of the 3α reaction (WCL) and the growing of the (C+O)/He ratio in the WCE and WO stars. The comparison of the observed and predicted abundance ratios confirms the validity of the views on the CNO cycle and He-burning.

The evolution of massive stars is highly dependent on the initial stellar metallicity Z through the effects of mass loss. The mass loss depends on metallicity because the radiation pressure on the envelope depends on the abundance of metallic ions (Heger et al. 2003). The mass loss $\dot{M}$ in O- and B-type stars varies like $\dot{M} \sim Z^\alpha$ with a value of α between 0.5 and 1. When the star enters the WNE stage and after the disappearance of its hydrogen, a very important effect is that its mass loss rates essentially behave like $\dot{M} \sim M^{2.5}$, probably with no dependence on the initial Z. Consequently, the $\dot{M}$-rates are very large at the beginning of the WNE stage (up to $10^{-2}M_\odot$/year

for $M \simeq 50M_{\odot}$) and they then decline very rapidly as the stellar mass is decreasing. This produces a remarkable mass convergence (for example, all stars at solar metallicity with initial $M \geq 25M_{\odot}$ reach the pre-SN stage with a final mass of about $5M_{\odot}$). The metallicity dependence of the mass loss rates has been included in various grids and models. As a result the relation between the final and initial masses is very different according to the initial Z. At solar Z one has the above-mentioned mass convergence, while at very low Z the final masses are very close to the initial ones.

The initial metallicity of the star affects not only mass loss, but also the outcome of nucleosynthesis. For metallicities $Z < Z_{\odot}/20$ mass loss has presumably a negligible effect on the yields of stars of all masses. During H-burning the initial CNO transforms to ^{14}N, and part of the latter nucleus turns into ^{22}Ne during He-burning (through α captures and one β decay). ^{12}C, ^{14}N and ^{16}O all have equal numbers of neutrons and protons but not ^{22}Ne (10 protons and 12 neutrons). This surplus of neutrons (increasing with initial metallicity) affects the products of subsequent burning stages and, in particular, of explosive burning, favoring the production of odd nuclei ("odd-even" effect) (Prantzos 2000).

Mass Loss Rates

- The mass loss rate employed during helium burning (up to carbon ignition) is $\dot{M} = -kM^{2.5}$ (with M in $M_{\odot}$ and $\dot{M}$ in $M_{\odot}$/year) and $k = 6 \times 10^{-8} M_{\odot}$/year, so long as the carbon surface mass fraction does not exceed 0.02, and $k = 10^{-7} M_{\odot}$/year afterward (Langer 1989b). This is also the mass loss rate taken for hydrogen-free WR phase, but with $k = 6 \times 10^{-8} M_{\odot}$/year (García-Segura et al. 1996).
- For WR stars with a nonvanishing surface hydrogen abundance (WNL stars) the mass loss might be assumed constant: $3 \times 10^{-5} M_{\odot}$/year for $M < 25M_{\odot}$, $5 \times 10^{-5} M_{\odot}$/year for $25M_{\odot} < M < 35M_{\odot}$ and $8 \times 10^{-5} M_{\odot}$/year for $M > 35M_{\odot}$ (Schmutz et al. 1989).
- For hydrogenless WR stars a mass loss rate as follows can be adopted:

$$\dot{M} = -k\left(\frac{M}{M_{\odot}}\right)^{\alpha}$$

with $\alpha = 2.6$, and $k = 5 \times 10^{-8} M_{\odot}$/year for hydrogenless WN stars (WNE stars) and $k = 10^{-7} M_{\odot}$/year for WC/WO stars (Langer 1989a).

7. Effects of Rotation on the Surface Abundances and Chemical Yields

For non-rotating stars, the surface enrichment in H and N occurs when the star reaches the RSG phase. There, CNO elements are dredged-up by deep convection. For rotating stars, N-excesses occur already during the MS phase, for solar metallicity $Z = 0.02$, the predicted excesses amount to factors 3 and 4 for initial v_{rot} =200 and 300 km/s respectively. At lower metallicity, the N-enrichment during the MS phase is smaller, due to the lower mass loss. However, there is a very large increase (up to a factor of ~ 10) for late B-type supergiants, because at low Z the star spends a lot of time in the blue phase and mixing processes have time to work. These predictions are in agreement with the observed excesses for galactic B- and A-type supergiants. Also the very large excesses observed for A-type supergiants in the Small Magellanic Cloud are remarkably well accounted for.

The chemical yields are strongly modified by rotation. The larger He-cores obtained in rotating models at core collapse imply larger productions of He and other α-nuclei elements. This is the most important effect of rotation on the chemical yields. In addition, by enhancing the mass loss rates and making the formation of WR stars easier, rotation favours the enrichment of the ISM by stellar winds.

The rotational diffusion during the H-burning phase enriched the outer layers in CNO processed elements. Some ^{14}N is extracted from the core and saved from further destruction. The same can be said for ^{17}O and ^{26}Al, a radioisotope with a half-life of 0.72 Myr. The mixing in the envelope of rotating stars also leads to a faster depletion of the temperature sensitive light isotopes, for instance lithium and boron (Fliegner et al. 1996). The supergiants at low Z in the range of 9 to 20 $M_{\odot}$ seem to be good candidates for the production of primary nitrogen (Maeder 2000).

8. Model

For computing the mass fractions of different elements in the winds of massive stars it is useful to write:

$$\bar{X_i} = \frac{\int_{M_i}^{M_f} X_i(M)\Phi(M)\dot{M}(X_i)dM}{\int_{M_i}^{M_f} \Phi(M)\dot{M}(X_i)dM} \quad (1)$$

where $X_i(M)$ are the compositions (see the Table 1) of the stellar wind ejecta for the element i (which can be H, He, C, etc.), for one computed stellar model (with given semiconvection and metallicity) and for one initial stellar mass.

Here $\Phi(M)$ is the Miller-Scalo IMF:

$$\Phi(\log M) = C_0 \exp\left[-C_1(\log M - C_2)^2\right]$$

where $C_0 = 66.2$, $C_1 = 1.15$, $C_2 = -0.88$. M is the mass of MS star in units of $M_{\odot}$.

In the equation (1), M_i and M_f are the initial and final masses between which the stars exploding as supernova enrich the ISM. For obtaining the contribution of all the masses from H-R diagram one must make a summation after all those intervals between 15 and 50 solar masses (so, for the stars that are having strong winds).

The mass range is split in intervals because in a representation $\log X_i = f(\log M)$:

1) There is no unique function to describe the evolution (in logarithmic scale) of the mass fractions as function of mass. In the first approximation, this evolution can be described by a step function. The reason for this behavior is that stars with different mass ranges have different wind mass losses and, so different contributions to the enrichment of ISM, and because the mechanism through which the wind is driven changes at 25-30 $M_{\odot}$;

Table 1. Surface mass fractions of various isotopes in stellar evolution models in the initial mass range $15M_\odot \leq M_{init} \leq 50M_\odot$ at the pre-SN stage. The pre-SN configuration is also indicated, where RSG means red supergiant and WC stands for Wolf-Rayet star of the carbon sequence. The last column gives the initial mass fractions used in the stellar evolution calculations (Langer & Henkel 1995).

	$15M_\odot$	$20M_\odot$	$25M_\odot$	$30M_\odot$	$40M_\odot$	$50M_\odot$	initial
isotop	RSG	RSG	RSG	RSG	WC	WC	
^{1}H	$6.75 \cdot 10^{-1}$	$6.48 \cdot 10^{-1}$	$6.31 \cdot 10^{-1}$	$6.16 \cdot 10^{-1}$	0.0	0.0	$7.00 \cdot 10^{-1}$
^{4}He	$3.06 \cdot 10^{-1}$	$3.32 \cdot 10^{-1}$	$3.49 \cdot 10^{-1}$	$3.65 \cdot 10^{-1}$	$7.22 \cdot 10^{-1}$	$1.49 \cdot 10^{-1}$	$2.80 \cdot 10^{-1}$
^{12}C	$2.40 \cdot 10^{-3}$	$2.00 \cdot 10^{-3}$	$2.05 \cdot 10^{-3}$	$2.01 \cdot 10^{-3}$	$2.07 \cdot 10^{-1}$	$4.94 \cdot 10^{-1}$	$3.48 \cdot 10^{-3}$
^{13}C	$1.04 \cdot 10^{-4}$	$2.08 \cdot 10^{-4}$	$1.35 \cdot 10^{-4}$	$1.39 \cdot 10^{-4}$	$4.70 \cdot 10^{-7}$	0.0	$3.87 \cdot 10^{-5}$
^{14}N	$3.04 \cdot 10^{-3}$	$4.17 \cdot 10^{-3}$	$4.42 \cdot 10^{-3}$	$4.83 \cdot 10^{-3}$	$4.51 \cdot 10^{-3}$	0.0	$1.03 \cdot 10^{-3}$
^{15}N	$2.27 \cdot 10^{-6}$	$2.05 \cdot 10^{-6}$	$1.69 \cdot 10^{-6}$	$1.62 \cdot 10^{-6}$	0.0	0.0	$3.77 \cdot 10^{-6}$
^{16}O	$9.09 \cdot 10^{-3}$	$8.21 \cdot 10^{-3}$	$7.85 \cdot 10^{-3}$	$7.42 \cdot 10^{-3}$	$4.81 \cdot 10^{-2}$	$3.32 \cdot 10^{-1}$	$9.98 \cdot 10^{-3}$
^{17}O	$5.69 \cdot 10^{-5}$	$6.04 \cdot 10^{-5}$	$6.46 \cdot 10^{-5}$	$6.95 \cdot 10^{-5}$	$8.33 \cdot 10^{-6}$	0.0	$3.80 \cdot 10^{-6}$
^{18}O	$1.18 \cdot 10^{-5}$	$3.33 \cdot 10^{-6}$	$8.67 \cdot 10^{-6}$	$8.22 \cdot 10^{-6}$	$8.92 \cdot 10^{-4}$	0.0	$2.00 \cdot 10^{-5}$
^{19}F	$3.26 \cdot 10^{-7}$	$3.44 \cdot 10^{-7}$	$2.73 \cdot 10^{-7}$	$2.53 \cdot 10^{-7}$	$0.03 \cdot 10^{-9}$	$0.05 \cdot 10^{-9}$	$3.74 \cdot 10^{-7}$
^{20}Ne	$1.70 \cdot 10^{-3}$	$1.70 \cdot 10^{-3}$	$1.70 \cdot 10^{-3}$	$1.70 \cdot 10^{-3}$	$1.68 \cdot 10^{-3}$	$1.66 \cdot 10^{-3}$	$1.70 \cdot 10^{-3}$
^{21}Ne	$3.93 \cdot 10^{-6}$	$3.90 \cdot 10^{-6}$	$3.28 \cdot 10^{-6}$	$3.05 \cdot 10^{-6}$	$1.38 \cdot 10^{-5}$	$3.61 \cdot 10^{-5}$	$4.14 \cdot 10^{-6}$
^{22}Ne	$1.10 \cdot 10^{-4}$	$1.00 \cdot 10^{-4}$	$9.77 \cdot 10^{-5}$	$9.43 \cdot 10^{-5}$	$1.21 \cdot 10^{-2}$	$1.84 \cdot 10^{-2}$	$1.24 \cdot 10^{-4}$
^{23}Na	$5.10 \cdot 10^{-5}$	$5.56 \cdot 10^{-5}$	$6.53 \cdot 10^{-5}$	$6.98 \cdot 10^{-5}$	$1.78 \cdot 10^{-4}$	$1.76 \cdot 10^{-4}$	$3.46 \cdot 10^{-5}$
^{24}Mg	$5.38 \cdot 10^{-4}$	$5.38 \cdot 10^{-4}$	$5.38 \cdot 10^{-4}$	$5.38 \cdot 10^{-4}$	$4.11 \cdot 10^{-4}$	$2.26 \cdot 10^{-4}$	$5.38 \cdot 10^{-4}$
^{25}Mg	$6.52 \cdot 10^{-5}$	$6.22 \cdot 10^{-5}$	$5.92 \cdot 10^{-5}$	$5.70 \cdot 10^{-5}$	$2.12 \cdot 10^{-4}$	$9.34 \cdot 10^{-4}$	$6.81 \cdot 10^{-5}$
^{26}Mg	$7.86 \cdot 10^{-5}$	$8.08 \cdot 10^{-5}$	$8.34 \cdot 10^{-5}$	$8.52 \cdot 10^{-5}$	$3.90 \cdot 10^{-4}$	$2.03 \cdot 10^{-3}$	$7.50 \cdot 10^{-5}$
^{26}Al	$0.25 \cdot 10^{-9}$	$5.22 \cdot 10^{-9}$	$9.07 \cdot 10^{-8}$	$2.99 \cdot 10^{-7}$	$4.09 \cdot 10^{-7}$	$3.60 \cdot 10^{-7}$	0.0
^{27}Al	$6.05 \cdot 10^{-5}$	$6.06 \cdot 10^{-5}$	$6.07 \cdot 10^{-5}$	$6.10 \cdot 10^{-5}$	$7.75 \cdot 10^{-5}$	$8.02 \cdot 10^{-5}$	$6.00 \cdot 10^{-5}$
^{28}Si	$6.80 \cdot 10^{-4}$	$6.80 \cdot 10^{-4}$	$6.80 \cdot 10^{-4}$	$6.80 \cdot 10^{-4}$	$5.59 \cdot 10^{-4}$	$3.63 \cdot 10^{-4}$	$6.80 \cdot 10^{-4}$
^{29}Si	$3.44 \cdot 10^{-5}$	$3.44 \cdot 10^{-5}$	$3.44 \cdot 10^{-5}$	$3.44 \cdot 10^{-5}$	$1.06 \cdot 10^{-4}$	$1.49 \cdot 10^{-4}$	$3.44 \cdot 10^{-5}$
^{30}Si	$2.28 \cdot 10^{-5}$	$2.28 \cdot 10^{-5}$	$2.28 \cdot 10^{-5}$	$2.28 \cdot 10^{-5}$	$7.86 \cdot 10^{-5}$	$2.43 \cdot 10^{-4}$	$2.28 \cdot 10^{-5}$
^{56}Fe	$1.32 \cdot 10^{-3}$	$1.32 \cdot 10^{-3}$	$1.32 \cdot 10^{-3}$	$1.32 \cdot 10^{-3}$	$1.32 \cdot 10^{-3}$	$1.32 \cdot 10^{-3}$	$1.32 \cdot 10^{-3}$

2) The composition in the wind between 15 and 25 $M_\odot$ is dominated by He, and between 25 and 50 $M_\odot$ by C and O.

The mass loss $\dot{M}_i$ for the element i (in $M_\odot$) is (Woosley et al. 1995):

$$\dot{M}(X_i) = \int X_{i,surf.}(t, M)\dot{M}(t, M)dt$$

Assuming that the mass loss is constant in time, the above equation will become (Woosley et al. 1995):

$$\dot{M}(X_i) = X_{i,surf.}(M) \cdot \dot{M}(M) = X_i(M) \cdot \dot{M}(M)$$

For practical reasons it is useful to put all these terms in a dependence as a function of $\ln M$ instead of M. Then, the equation (1) can be rewritten:

$$\bar{X_i} = \frac{\int_{\ln M_i}^{\ln M_f} X_i^2(M)\Phi(M)M\dot{M}(M)dM}{\int_{\ln M_i}^{\ln M_f} X_i(M)\Phi(M)M\dot{M}(M)dM} \quad (2)$$

where we introduced the expression for $\dot{M}_i$ and we assumed that $X_i \approx X_{i,surf}$.

We will have $X_i(\ln M) = \exp(\mathcal{F})$ where $\mathcal{F} = a \ln M + b$ is the fitting function for $\ln X_i = f(\ln M)$ for the domain in which is the integral is defined.

$$\Phi(\ln M) = \exp[\ln C_0 - C_1(0.434 \cdot \ln M - C_2)^2] \quad (3)$$

$\dot{M} = \exp(\mathcal{G})$, where $\mathcal{G} = \exp(\ln k + \alpha \ln M)$, with k and α given into the section 6. $\mathcal{G}$ can be taken as the logaritmic of some numerical value given for the assumed stellar evolution model, for the stellar mass range in which is done the integration and, most important, for the considered element.

Introducing all this functions into the integral we can compute the mass fractions in the wind.

In order to obtain the mass fractions in CR it is necessary to compute the ratios between the observed cosmic rays and, also, the mass fractions from our proposed model for one example. In this way it can be seen the general form and, also, some particularization for the formulas.

Plotting the data of individual nuclei as provided by the direct experiments so far shows, in general, a fair correspondence in overlapping energy ranges. The spectra can be described by simple power laws in energy:

$$\phi = \phi_0 E^{-\gamma}$$

where ϕ is the integral differential flux in particles/(m^2 s sr TeV/nucleus), ϕ_0 are the absolute flux normalizations and γ the spectral index for various elements. The fitting was done by Wiebel-Sooth & Biermann. Their results for elements between H and Ni can be seen in the table 2.

In Fig. 2 the abundances of the various nuclei at 1 TeV (Wiebel-Sooth et al. 1998), for the elements up to Fe as well as the lower energy data for ultra-heavy nuclei beyond the iron group are compared to the solar system abundances.

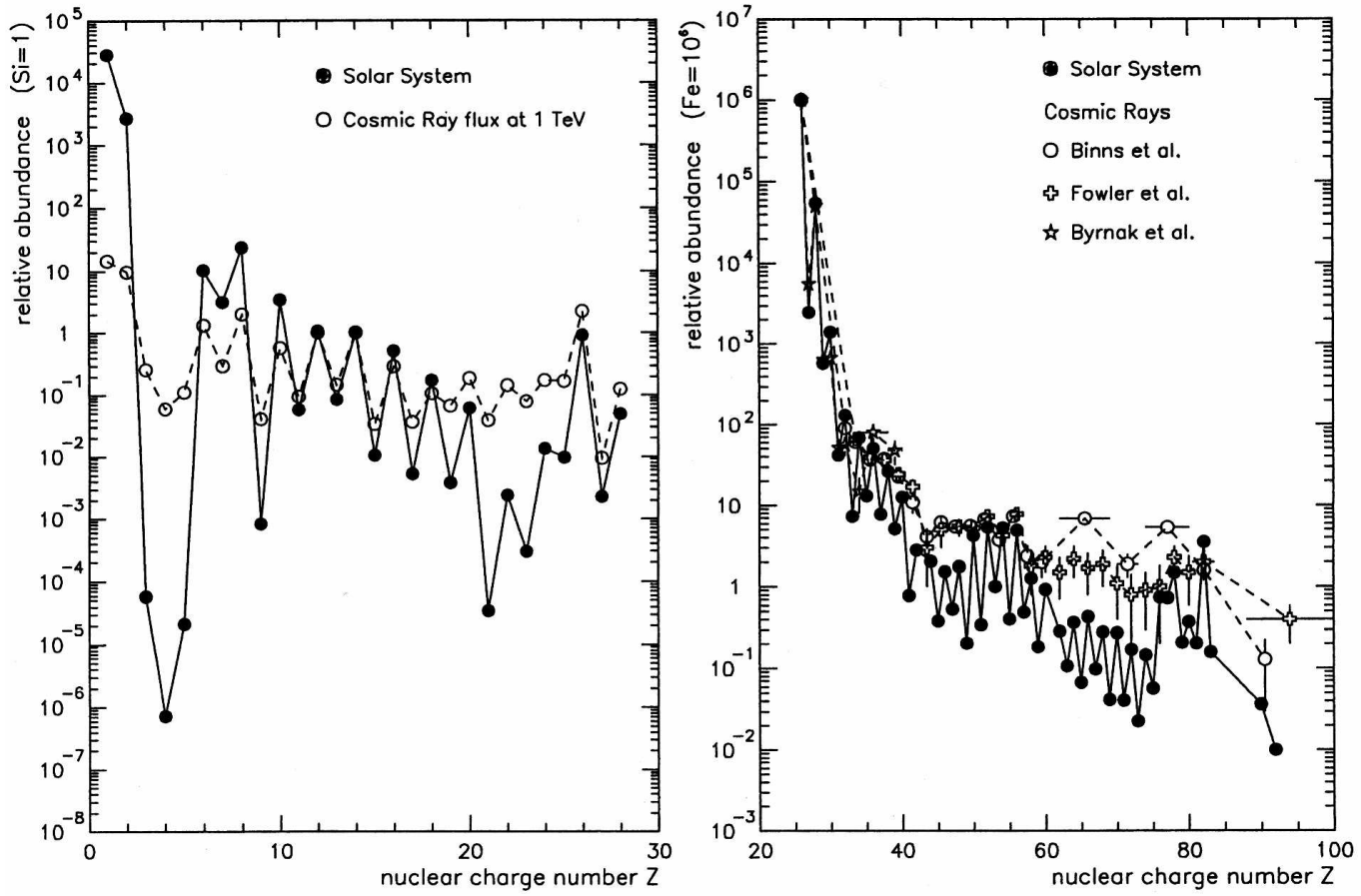

Fig. 2. The abundances of various nuclei in the cosmic radiation compared to the abundances of the elements in the solar system. (a) The elements H - Ni (normalized to Si=1, cosmic ray flux at 1 TeV/nucleus). (b) The elements Fe - Fm (normalized to Fe=10^6, cosmic ray flux > 1.5 GeV/nucleon) (Wiebel-Sooth et al. 1998; Grevesse & Anders 1989).

In the particular case of, let say, carbon:

$$\phi_{0,C} = \phi_{0,^{12}C} + \phi_{0,^{13}C} \quad (4)$$

where:

$$\gamma_{^{12}C} = \gamma_{^{13}C} = \gamma_C$$

From (4):

$$N_C(E) = N_{^{12}C}(E) + N_{^{13}C}(E)$$

which, in the general case, will look like (j is for the isotopes):

$$N_{sum,i}(E) = \sum_j N_{ij}(E)$$

with:

$$N^{observed}_{sum,i}(E) \simeq N^{CR}_{sum,i}(E)$$

Then, taking the minimum energy at a given rigidity p^*_i/Z and considering that is not existing one superior limit for energy at which the particle can be accelerated, we will have the number of particles of one type of the form:

$$N_i^{observed} = \int_{E^*} N^{theor}_{sum,i}(E)dE$$

$$N_i^{observed} = \int_{p_i^*} \phi_{0,i}\left(\frac{pc}{E_0}\right)^{-\gamma} d\left(\frac{pc}{E_0}\right)$$

$$N_i^{observed} = \phi_{0,i}\frac{1}{\gamma_i - 1}\left(\frac{p_i^* c}{E_0}\right)^{1-\gamma_i}$$

Now, because the mass fraction:

$$X_i = \frac{N_i m_i}{\sum_k N_k m_k}$$

with k=H,..,i,...,Fe , the observed cosmic ray ratio between mass fractions will be (for carbon):

$$\frac{X_C}{X_{He}} = \frac{N_C^{CR} m_C}{N_{He}^{CR} m_{He}}$$

or, introducing N_C^{CR} and N_{He}^{CR} in the above formula:

Table 2. The spectral indices γ and absolute flux normalization ϕ_0 for the various elements with nuclear charge number Z. We can see that the spectral index for Hydrogen is close to 2.74, and for all the other elements (except Li, Be and B which are spallation products) it is close to 2.67 (Wiebel-Sooth et al. 1998).

Element	Z	ϕ_0 [m^2 s sr TeV/nucleus] $^{-1}$	γ	$\frac{\chi^2}{df}$
H	1	$(10.57 \pm 0.30) \cdot 10^{-2}$	2.76 ± 0.02	0.70
He	2	$(6.73 \pm 0.20) \cdot 10^{-2}$	2.63 ± 0.02	2.10
Li	3	$(2.08 \pm 0.51) \cdot 10^{-3}$	2.54 ± 0.09	0.90
Be	4	$(4.74 \pm 0.48) \cdot 10^{-4}$	2.75 ± 0.04	0.37
B	5	$(8.95 \pm 0.79) \cdot 10^{-4}$	2.95 ± 0.05	0.45
C	6	$(1.06 \pm 0.01) \cdot 10^{-2}$	2.66 ± 0.02	1.42
N	7	$(2.35 \pm 0.08) \cdot 10^{-3}$	2.72 ± 0.05	1.91
O	8	$(1.57 \pm 0.04) \cdot 10^{-2}$	2.68 ± 0.03	1.70
F	9	$(3.28 \pm 0.48) \cdot 10^{-4}$	2.69 ± 0.08	0.47
Ne	10	$(4.60 \pm 0.10) \cdot 10^{-3}$	2.64 ± 0.03	3.14
Na	11	$(7.54 \pm 0.33) \cdot 10^{-4}$	2.66 ± 0.04	0.36
Mg	12	$(8.01 \pm 0.26) \cdot 10^{-3}$	2.64 ± 0.04	0.10
Al	13	$(1.15 \pm 0.15) \cdot 10^{-3}$	2.66 ± 0.04	1.24
Si	14	$(7.96 \pm 0.15) \cdot 10^{-3}$	2.75 ± 0.04	0.10
Mn	25	$(1.35 \pm 0.14) \cdot 10^{-3}$	2.46 ± 0.22	5.38
Fe	26	$(1.78 \pm 0.18) \cdot 10^{-2}$	2.60 ± 0.09	1.81

$$\frac{X_C}{X_{He}} = \frac{\phi_{0,C} \frac{1}{\gamma_C - 1} \left(\frac{p^*_C c}{E_0}\right)^{1-\gamma_C}}{\phi_{0,He} \frac{1}{\gamma_{He} - 1} \left(\frac{p^*_{He} c}{E_0}\right)^{1-\gamma_{He}}} \frac{m_C}{m_{He}} \tag{5}$$

formula which can be simplified using the rigidity $\frac{p^*_C}{Z_C} = \frac{p^*_{He}}{Z_{He}}$:

$$\frac{X_C}{X_{He}} = \frac{\phi_{0,C}}{\phi_{0,He}} \frac{\gamma_{He} - 1}{\gamma_C - 1} \left(\frac{Z_C}{Z_{He}}\right)^{1-\gamma_C} \left(\frac{p^*_{He} c}{E_0}\right)^{\gamma_{He} - \gamma_C} \frac{m_C}{m_{He}} \tag{6}$$

In the equation (6), $p^{*2}_{He} = \sqrt{2 m_{He} E_0}$, with $E_0 = 100 MeV$ the lower energy cutoff.

The cosmic ray ratio between mass fractions will be:

$$\frac{X_C}{X_{He}} = \frac{X_{^{12}C} + X_{^{13}C}}{X_{He}}$$

The general formulation of the above relation being:

$$\frac{X_i}{X_{He}} = \frac{\sum_j X_{ij}}{X_{He}}$$

In our model, for obtaining the real mass fractions in CR it is also necessary the introduction of FIP correction factors (to make possible the consideration of ionization losses):

$$\frac{X_i}{X_{He}} = \frac{\sum_i X_i}{X_{He}} \cdot I_{element}$$

In this way the value for ratios of mass fractions of any element present in cosmic rays and He can be computed and, after that, compared with those results given by the model for the same ratios.

9. Results

After several tests we saw that the stellar mass loss was just a second order correction in the obtained results, so, it was possible to excluded it from the equations. In this way, the model mass fraction formula (2) becomes:

$$\overline{X_i} = \frac{\int_{\ln M_i}^{\ln M_f} X_i^2(M) \Phi(M) M dM}{\int_{\ln M_i}^{\ln M_f} X_i(M) \Phi(M) M dM} \tag{7}$$

For the correctitude of our computation we had to consider also that the mass fractions in the wind are constant between two mass values. All the other terms in the above formulas where relevant to our computations.

First, the mass fractions for RSG and WR stars were considered to have an equal contribution to the production of the observed cosmic radiation. For this case, the obtained values are summarized in the table 3 where, in the second column is the nuclear charge number, in the third the mass number. The column noted with FIP is containing the first ionization potential for the considered element. In the ninth column we are having the factor that is needed for the equality of the model and cosmic ray abundances, each normalized to the corresponding mass fraction for helium. *min.* and *max.* are the factors with which we must multiply the model mass fraction ratios in order to take account also of the spallation correction ratios and to obtain the experimental value.

$$min. \times \left(\frac{X_i}{X_{He}}\right)^{model} \leq \left(\frac{X_i}{X_{He}}\right)^{observed} \leq max. \times \left(\frac{X_i}{X_{He}}\right)^{model}.$$

We will try to prove that, after considering the spallation correction, the factor that separates the model mass fraction ratios from the observed ones (for even-Z elements) is related to the ionization losses, meaning abundance decrease, for elements whose FIP exceeds about 10 eV, due to the particle escape mechanism from the photosphere and the chromosphere to corona, and,also, to the diferentiated radiative preacceleration (before the shock injection) between different species of WR star wind particles. Proving that the radiative acceleration plays an important role in the abundance of cosmic rays will be an independent study and, because of its complexity, will make the subject of another paper.

Analyzing the data in the table 3 we see that, first, the mass fractions in the column 4 are too high. In the second place, the columns 10 and 11 factors are not even allowing the spallation correction for even-Z elements (see O, Ne,Si) and, also, no FIP correction factor (see column 9) is evident for the elements with FIP$\geq$ 10 eV. Also, we can not count for a correct value for the observed cosmic ray hydrogen in this theoretical interpretation because its principal contribution to the interstellar medium enrichment and cosmic ray spectrum comes not from stars with $15 M_\odot \leq M \leq 50 M_\odot$ but from other sources: low mass stars (ISM SNe and RSG SNe) and Active Galactic Nuclei (AGN) jets.

So, it is necessary to consider that the WR and RSG stars are having a different contribution to the element abundance in CRs. The formula which describes this can be written:

Table 3. Our model data considering that RSG and WR stars are having an equal contribution to the production of the observed cosmic radiation

elem.	Z	A	$\bar{X}_{i,RSG}^{model}$	$\bar{X}_{i,WR}^{model}$	$\bar{X}_{i}^{model}$	$\left(\frac{\bar{X}_i}{X_{He}}\right)^{model}$	FIP [eV]	factor model/observed	min. (for $\gamma_{observed}$)	max. (for $\gamma_{observed}$)
H	1	2	-	-	-	1.364058	13.6	1/1.42	5.33	-
He	2	4	$6.45098 \cdot 10^{-1}$	$1.31679 \cdot 10^{-1}$	$7.7052 \cdot 10^{-1}$	1	24.4	-	-	-
C	6	12	$4.22546 \cdot 10^{-3}$	$3.77525 \cdot 10^{-2}$	$4.19782 \cdot 10^{-2}$	0.05448	11.27	$1/(1.42 \cdot 43)$	1	2
N	7	14	$7.45885 \cdot 10^{-3}$	$8.22535 \cdot 10^{-2}$	$8.97124 \cdot 10^{-2}$	0.11643	14.52	1/43	1	2
O	8	16	$1.6265 \cdot 10^{-2}$	$8.7725 \cdot 10^{-3}$	$2.50375 \cdot 10^{-2}$	0.03249	13.56	1	1	~ 1
F	9	19	$5.99832 \cdot 10^{-7}$	$5.47141 \cdot 10^{-12}$	$5.99837 \cdot 10^{-7}$	$7.7848 \cdot 10^{-7}$	17.4	$15 \div 20$	1	2
Ne	10	20	$3.29658 \cdot 10^{-3}$	$3.06398 \cdot 10^{-4}$	$3.60298 \cdot 10^{-3}$	$4.676 \cdot 10^{-3}$	21.48	1	1	~ 1
Na	11	23	$1.11809 \cdot 10^{-4}$	$3.24637 \cdot 10^{-5}$	$1.44272 \cdot 10^{-4}$	$1.8724 \cdot 10^{-4}$	5.14	1	0.97	1
Mg	12	24	$1.04327 \cdot 10^{-3}$	$7.49583 \cdot 10^{-5}$	$1.11823 \cdot 10^{-3}$	$1.4513 \cdot 10^{-3}$	7.64	1	0.62	1
Al	13	27	$1.17598 \cdot 10^{-4}$	$1.41344 \cdot 10^{-5}$	$1.31733 \cdot 10^{-4}$	$1.7096 \cdot 10^{-4}$	5.98	1	0.55	1
Si	14	28	$1.31863 \cdot 10^{-3}$	$1.01951 \cdot 10^{-4}$	$1.42058 \cdot 10^{-3}$	$1.8436 \cdot 10^{-3}$	8.15	1	1	~ 1
Fe	26	56	$2.5597 \cdot 10^{-3}$	$2.40742 \cdot 10^{-4}$	$2.80044 \cdot 10^{-3}$	$3.6345 \cdot 10^{-3}$	7.90	20	1	2

$$\bar{X}_i^{model} = \alpha \bar{X}_{i,RSG}^{model} + (1-\alpha)\bar{X}_{i,WR}^{model} \quad (8)$$

where, for the above case we had $\alpha = 1/2$.

In the same time we need the one formula that is giving the radiative preacceleration correction in the stellar wind and which, after the introduction of the spallative correction, to give an overabundance in the wind (for Mg, Si and Fe), relative to the observed CRs, situated between 4 and 6 (if we are taking 1 as reference level for *CR/surface* abundaces for C, O and Ne).

To make it more clear it may be necessary to say that, for a FIP correction "hidden" in the mass fraction ratio, *observed/model* it is the same as saying instead *CR/surface*.

At first, the form of this preacceleration correction equation has been taken as being:

$$\left(\frac{\bar{X}_i}{X_{He}}\right)^{observed} \simeq \left(\frac{Z_i}{Z_{He}}\right)^{\gamma_{inj.}-1} \frac{A_{He}}{A_i} \left(\frac{\bar{X}_i}{X_{He}}\right)^{model} . \quad (9)$$

In this way:

$$\left(\frac{\bar{X}_i}{X_{He}}\right)^{observed} = \left(\frac{Z_i}{Z_{He}}\right)^{\gamma_{inj.}-1} \frac{A_{He}}{A_i} \frac{\alpha \bar{X}_i^{model,RSG} + (1-\alpha)\bar{X}_i^{model,WR}}{\alpha \bar{X}_{He}^{model,RSG} + (1-\alpha)\bar{X}_{He}^{model,WR}},$$

where $\left(\frac{\bar{X}_i}{X_{i,He}}\right)^{observed}$ must be equal with the observed flux at 1 TeV:

$$\left(\frac{\bar{X}_i}{X_{i,He}}\right)^{observed} = \left(\frac{\phi_{0,i}}{\phi_{0,He}}\right)^{observed} .$$

In the above equations $\gamma_{inj.}$ is the spectral index at injection into the SN shock.

After computations it was visible that, no matter what choice we were doing for the α parameter, the data obtained for *min.*, *max.* and *model/observed* were not in the limits gived by the physics hidden in these factors ($min \geq 0.5$ and $1.6 \leq max \leq 2$).

Further tries with some others forms for (9) gave no good results either (even using instead of $\gamma_{inj.} = 8/3$ the γ values from table 2).

The formula which worked was:

$$\left(\frac{\bar{X}_i}{X_{He}}\right)^{observed} \simeq \left(\frac{Z_i}{Z_{He}}\right)^{s} \left(\frac{\bar{X}_i}{X_{He}}\right)^{model} ,$$

where s is one parameter that was determined as being ~ 1 (see table 4). The signification of the factor $\left(\frac{Z_i}{Z_{He}}\right)^s$ seems to be related with a different preacceleration (and, consequently, a phase space separation) of the wind particles before their injection into the supernova shock of the WR predecessor.

In (8), trying $\alpha = 2/3$ (the contribution for RSG will be 66% and for WR 33%), we obtained for even-Z elements the values in the table 4.

Using other α factors we obtained also good results for $\alpha = 3/4$, $\alpha = 4/5$ and $\alpha = 3/5$ (see tables 5, 6 and 7).

Table 5. Mass fraction ratios for even-Z elements in the case that $\alpha = \frac{3}{4}$ and the preacceleration correction factor is $\left(\frac{Z_i}{Z_{He}}\right)^s$. The others columns that are missing from this table are similar with the ones from the table for $\alpha = \frac{2}{3}$

elem.	Z	$\left(\frac{\bar{X}_i}{X_{He}}\right)^{model}$	s	factor observed/model
H	1	-	-	$0.9715 \div 1.0912$
C	6	0.02439	1.041 ± 0.022	1
O	8	0.02785	1.022 ± 0.0265	1
Ne	10	$4.9329 \cdot 10^{-3}$	1.142 ± 0.022	1
Mg	12	$1.5505 \cdot 10^{-3}$	1	5.4399 ± 1.4418
Si	14	$1.9632 \cdot 10^{-3}$	1	3.6154 ± 0.9561
Fe	26	$3.8316 \cdot 10^{-3}$	1	2.2071 ± 0.8492

Table 4. Mass fraction ratios for even-Z elements in the case that $\alpha = \frac{2}{3}$ and the preacceleration correction factor is $\left(\frac{Z_i}{Z_{He}}\right)^s$

elem.	Z	$\left(\frac{\bar{X}_i}{X_{He}}\right)^{model}$	$\left(\frac{\bar{X}_i}{X_{He}}\right)^{observed}$	s	factor observed/model	χ^2
H	1	-	0.105 ± 0.075	-	$0.9936 \div 1.1161$	-
C	6	0.03278	0.035 ± 0.015	0.876 ± 0.022	1	1 ± 0.1
O	8	0.0293	0.045 ± 0.025	0.998 ± 0.0265	1	1.75 ± 0.55
Ne	10	$4.8955 \cdot 10^{-3}$	$(2.22 \pm 1.57) \cdot 10^{-2}$	1.145 ± 0.022	1	0.75 ± 0.02
Mg	12	$1.5336 \cdot 10^{-3}$	$\geq 5.8 \cdot 10^{-3}$	1	6.945 ± 2.936	-
Si	14	$1.9436 \cdot 10^{-3}$	$(5 \pm 2) \cdot 10^{-3}$	1	4.6828 ± 2.02	-
Fe	26	$3.8032 \cdot 10^{-3}$	$\geq 3.05 \cdot 10^{-3}$	1	3.1156 ± 1.7623	-

Table 6. Mass fraction ratios for even-Z elements in the case that $\alpha = \frac{4}{5}$ and the preacceleration correction factor is $\left(\frac{Z_i}{Z_{He}}\right)^s$. The others columns that are missing from this table are similar with the ones from the table for $\alpha = \frac{2}{3}$

elem.	Z	$\left(\frac{\bar{X}_i}{X_{He}}\right)^{model}$	s	factor observed/model
H	1	-	-	$0.956 \div 1.0738$
C	6	0.02015	1.148 ± 0.022	1
O	8	0.02722	1.033 ± 0.0265	1
Ne	10	$4.9751 \cdot 10^{-3}$	1.138 ± 0.022	1
Mg	12	$1.5663 \cdot 10^{-3}$	1	5.2662 ± 1.3628
Si	14	$1.9824 \cdot 10^{-3}$	1	3.4966 ± 0.9014
Fe	26	$3.864 \cdot 10^{-3}$	1	2.1234 ± 0.801

Table 7. Mass fraction ratios for even-Z elements in the case that $\alpha = \frac{3}{5}$ and the preacceleration correction factor is $\left(\frac{Z_i}{Z_{He}}\right)^s$. The others columns that are missing from this table are similar with the ones from the table for $\alpha = \frac{2}{3}$

elem.	Z	$\left(\frac{\bar{X}_i}{X_{He}}\right)^{model}$	s	factor observed/model
H	1	-	-	$1.0334 \div 1.1607$
C	6	0.04011	0.764 ± 0.022	1
O	8	0.03017	0.984 ± 0.0265	1
Ne	10	$4.7768 \cdot 10^{-3}$	1.156 ± 0.022	1
Mg	12	$1.4917 \cdot 10^{-3}$	1	8.7264 ± 4.7126
Si	14	$1.892 \cdot 10^{-3}$	1	5.9638 ± 3.3042
Fe	26	$3.7116 \cdot 10^{-3}$	1	4.2764 ± 2.937

There were done computations also for α equal with 1/3, 1/4 and 1, but the differences between the *s* values for the triplet C, O and Ne were to big too consider any of these as a valid candidate for the exponent of Z.

By comparing the ratios *observed/model* from the tables 4, 5, 6 and 7 it can be remarked that, for Mg, Si and Fe the values which are entering in the domains of all three are for α=2/3 (*observed/model*=4.0088 ÷ 4.878) and for α=3/5 (*observed/model*=4.01385 ÷ 7.2134). Taking C, O and Ne mass fractions as reference ratios for *CR/surface* and equal to 1, we can see that the behaviour of this ratio versus FIP is having a very good resemblance with the ratio *CR/GA* described in "The FIP Factor Correction" section of this report. We must remember the fact that, from theoretical point of view, it is predicted that for the elements Mg, Si and Fe this factor must be the same (fig. 1). One confirmation of our α choices comes from the fact that it is known from other theoretical and observational sources that the hydrogen mass fraction is 3 ÷ 4 times less than the total CRs hydrogen mass fraction (in this energy range). This is the reason why, in the third column of the tables 4 - 7, the ratio $\left(\frac{\bar{X}_i}{X_{He}}\right)^{model}$ is so high. The FIP for hydrogen is 13.6 eV, making from it an element affected by ionization loss and placing it on the same underabundance (compared with the elements with FIP≤ 10 eV) level with Mg, Si and Fe. But, in both α=2/3 and α=3/5 the *observed/model* factor for H is fitting the theory by being at least 3 or 4 times smaller than the one for Mg, Si and Fe.

Each one of the our two α cases is having its good and bad sides. For α=2/3 we are having the smallest difference in *s* for C, O and Ne, but the sum over all the mass fractions for this α is bigger than the one for α=3/5, this sum being closer to 1 for the last case ($\simeq$ 1.2379 for α=2/3, and $\simeq$ 1.1065 for α=3/5); (see also the representation of the working cases for α values presented above - fig. 3, - fig. 4). The final choice can be made by testing the ^{22}Ne/^{20}Ne and (^{25}Mg+^{26}Mg)/^{24}Mg CRs ratios for both alphas.

10. Test

Neon is one of the most important elements in CRs because its two major isotopes, ^{22}Ne and ^{20}Ne, are formed by different processes of nucleosynthesis (^{23}Na(p, α)^{22}Ne; ^{16}O(α, γ)^{20}Ne; ^{14}N(α, γ)^{18}F(e$^+\nu$)^{18}O(α, γ)^{22}Ne). One neon component measured in carbonaceous chondrites meteorites, called neon-A, is believed to represent the primordial neon isotopic abundance at the formation of the solar system, and this value has been adopted as "standard" solar system composition: ^{22}Ne/^{20}Ne=0.122 ± 0.006

The abundance of ^{22}Ne/^{20}Ne measured for the galactic CR at the orbit of Earth is 0.54±0.07. Using standard solar modulation and others cosmic ray propagation models, the CR source ratio inferred is ^{22}Ne/^{20}Ne=0.38±0.07 (^{20}Ne/^{22}Ne=2.6±0.5) (Garcia-Munoz et al. 1979).

In our model for production and propagation of galactic CRs the ratio ^{22}Ne/^{20}Ne for α=2/3 is equal to 0.3777, in very good concordance with the given above source ratio. For

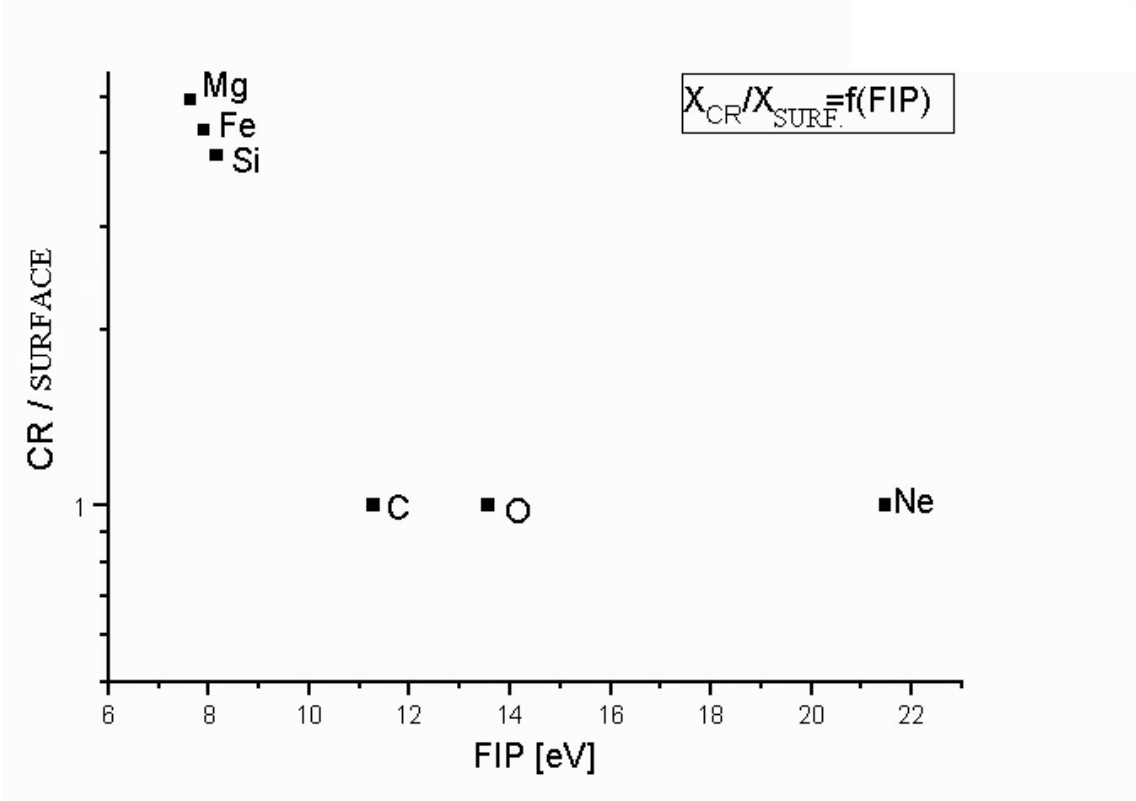

Fig. 3. The ratio of CRs mass fractions to the stellar surface mass fractions, corrected for spallation and transport in the ISM. Here α is 2/3

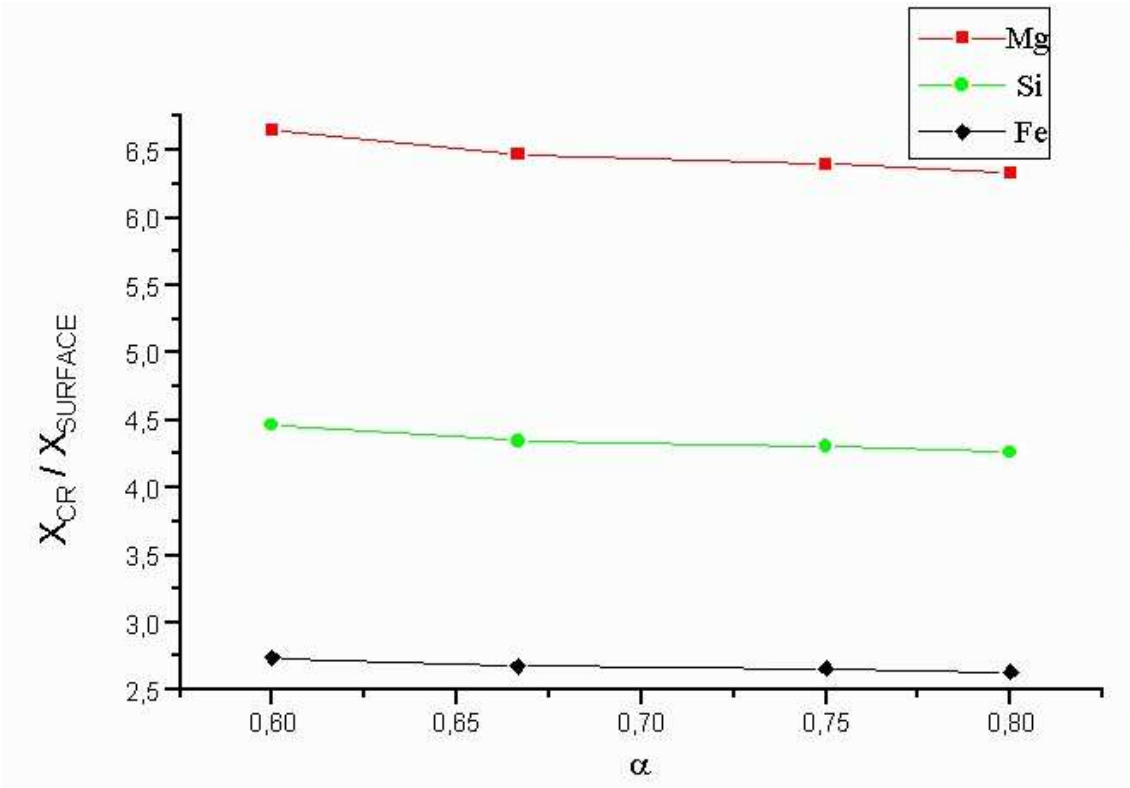

Fig. 4. The ratio of CRs mass fractions to the stellar surface mass fractions for Mg, Si and Fe, corrected for spallation and transport in the ISM, as function of α.

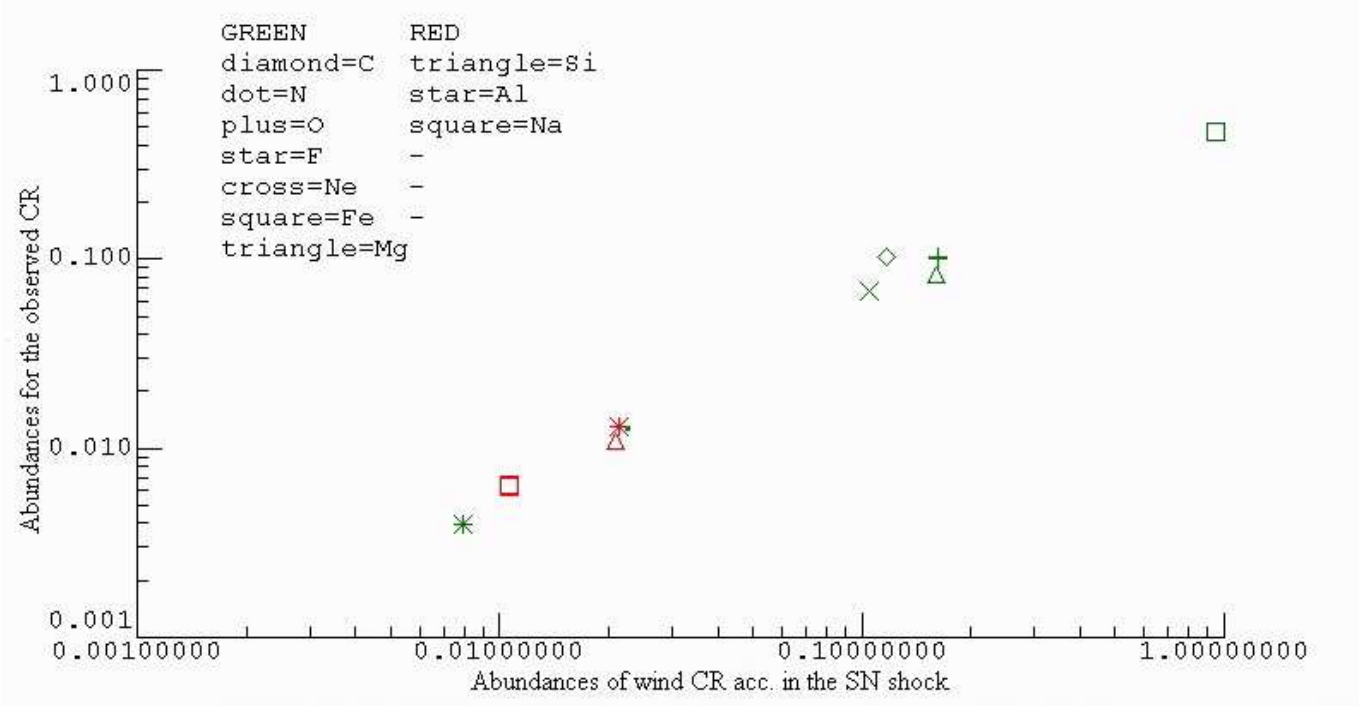

Fig. 5. The ratio of CRs mass fractions to He mass fraction as function of the ratio for the same element mass fractions to He mass fraction but computed in our model.

α=3/5 this ratio is 0.4772, larger than the CRs source ratio. We also found that (^{25}Mg+^{26}Mg)/^{24}Mg= 0.3076 (for α=2/3) and 0.3208 (for α=3/5)compared with the solar system value of 0.27, suggesting that the cosmic ray source and solar system material were synthesized under different conditions. The obtained values are also suggesting that α=2/3 is the right proportion.

11. Conclusions

- The observed cosmic ray radiation at energy up to $3 \cdot 10^{18}$ eV can be generated by acceleration of stellar wind particles in supernova shock (see fig. 5).
- The contribution ratio of RSG stars and WR stars to the CRs mass fractions is 2:1.
- Ionization loss is responsable for the underabundance in the observed CR elements with FIP≥ 10 eV.
- We can consider Si as reference element for overabundance of elements with FIP ≤ 10 eV relative to those affected by ionization loss (see fig. 3). The FIP correction factor will be, in this case, 4.4434 ± 0.4346. In this way, we can see that the elements with FIP less than 10 eV are having an larger mass fraction than the elements with FIP greater than 10 eV (relative to Si), by a factor of ∼ 4. This happens to be exactly $Z^2_{injection}$, the initial degree of ionization squared. Therefore, cosmic ray particles of an element with an initial degree of ionization of $Z^2_{injection}$ are more likely to be injected into the supernova shock.
- The observed cosmic rays have an increased mass fraction by another factor of $\left(\frac{Z_i}{Z_{He}}\right)^s$. This factor seems to be the result of a differentiated radiative preacceleration (phase space dispertion), before shock injection, of different elements found in the Wolf-Rayet stellar atmospheres. The reasons which are taking us to this conclusion will be detailed in another paper.

Acknowledgements. For this study we used the programming tool **O-Matrix 5.2**, a very powerfull and fast programming language. The code has many versions, as function of the intended goal, some parts of it being (in many of the versions) separated from the all in intention to obtain the manner in which are reacting some terms from the used equations. The complete code is having parts made under **Borland Delphi 5**.

References

Donea, A.C., Biermann, P.L., 1996, A&A, 1996, 316, 43.
Drury, L.O'C., Duffy, P., Eichler, D., Mastichiadis, A., 1999, A&A, 347, 370.
Drury, L.O'C., van der Swaluw, E., Carroll, O., 2003, http://arXiv/astro-ph/0309820.
Fliegner, J., Langer, N., Venn, K.A., 1996, A&A, 308, L13.
Garcia-Munoz, M., Simpson, J.A., Wefel, J.P., 1979, ApJ, 232, L95-L99.
García-Segura, G., Langer, N., Mac Low, M.-M., 1996, A&A, 316, 133-146.

Grevesse, N., Anders, E., 1989, in AIP Conference Proceedings 183: Cosmic Abundance in Matter, p. 1-7, American Institute of Physics.
Heger, A., Langer, N., 1996, A&A, 315, 421-431.
Heger, A., Fryer, C.L., Woosley, S.E., Langer, N., Hartmann, D.H., 2003, ApJ, 591, 288.
Langer, N., 1989a, A& A, 220, 135.
Langer, N., 1989b, A&A, 220, 135.
Langer, N., Henkel, C., 1995, Space Sci. Rev., 74, 343.
Lu, Y., Zhao, G., Deng, L.C., et al., 2001, A& A, 367, 277-281.
Maeder, A., 2000, New Astron. Rev., 44, 291-296.
Mastichiadis, A., 1996, A&A, 305, 53.
Meyer, J.-P., Drury, L.O'C., Ellison, D.C., 1997, ApJ, 487, 182.
Biman, B., Biermann, P.L., 1994, MNRAS, 267, 447.
Prantzos, N., 2000, New Astron. Rev., 44, 303-313.
Prantzos, N., Arnould, M., Arcoragi, J.P., Casse, M., 1985, in 19th Internat. Cosmic Ray Conf.(La Jolla), 3, 167.
Protheroe, R.J., 1996, in Towards the Millennium in Astrophysics: Problems and Prospects (Erice), Origin and Propagation of the Highest Energy Cosmic Rays, eds. M.M. Shapiro and J.P. Wefel (World Scientific).
Reynolds, S.P., 1996, ApJ, 459, L13.
Schmutz, W., Hamann, W.-R., Wessolowski, U., 1989, A&A, 210, 236.
Silberberg, R., Tsao, C.H., 1990, ApJ, 352, L49 - L52.
Tsao, C. H., Silberberg, R., Barghouty, A. F., 1998, ApJ, 501, 920-926.
Wiebel-Sooth, B., Biermann, P.L., Meyer, H., 1998, A&A, 330, 389-398.
Woosley, S.E., Langer, N., Weaver, T.A., 1995, ApJ, 448, 315.
Zirakashvili, V.N., Breitschwerdt, D., Ptuskin, V.S., Völk, H.J., 1996, A&A, 311, 113.